Supplemental Information

This PDF file includes: 1) supplemental figures S1 to S14, and 2) supplemental tables S1 to S4.

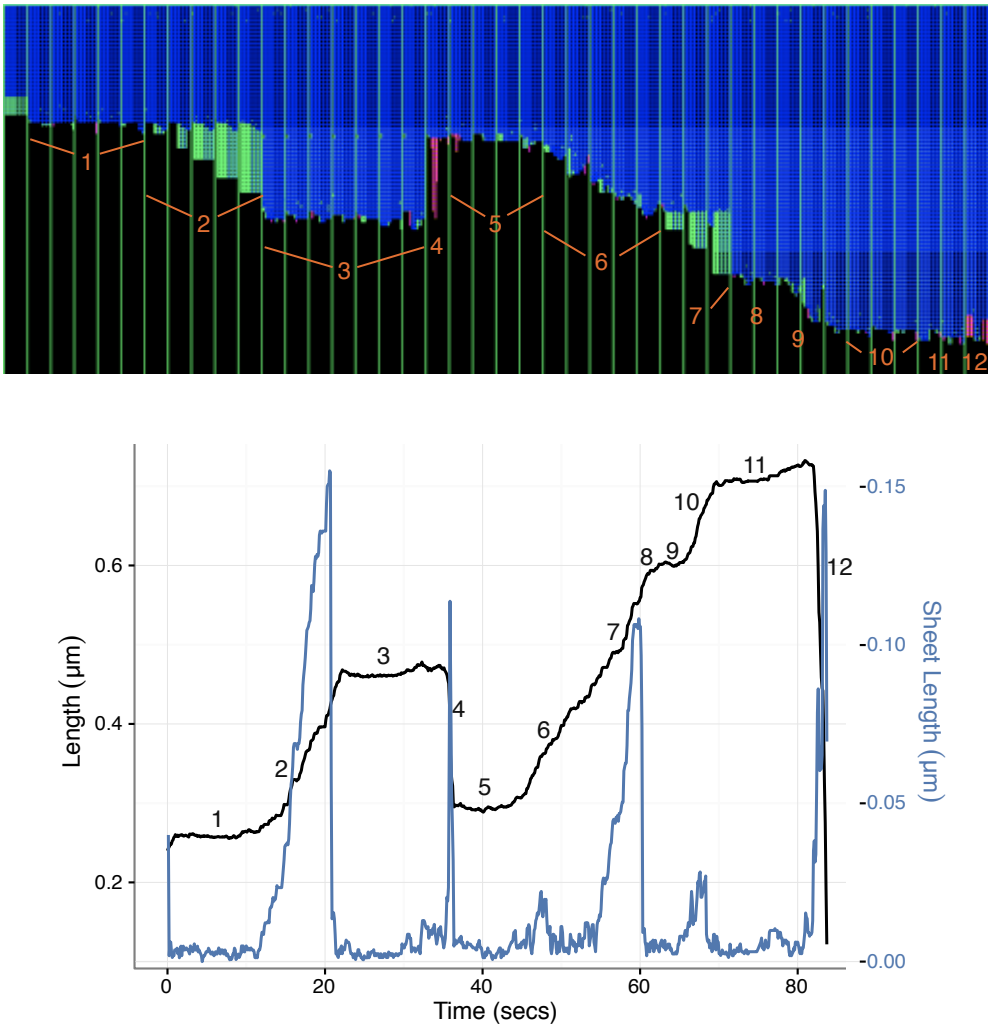

Figure S1: A trajectory showing different phases of dynamic instability. (**a**) The montage of lattice states in the trajecotry. In the montage, the color scheme is: Blue for interfaces (longitudinal or lateral) or monomers in S form; Green for interfaces or monomers in B form; Magenta for monomers in C form; Orange for longitudinal interaces in C form. (**b**) Different events and phases in the trajectory are marked in the montage. 1, 3, 8 and 11 indicate pausing during growth; 2, 7 and 9 indicate growth in sheet; 4 and 12 indicates catastrophe; 5 indicates pausing during shortening; 6 and 10 indicate growth in tube.

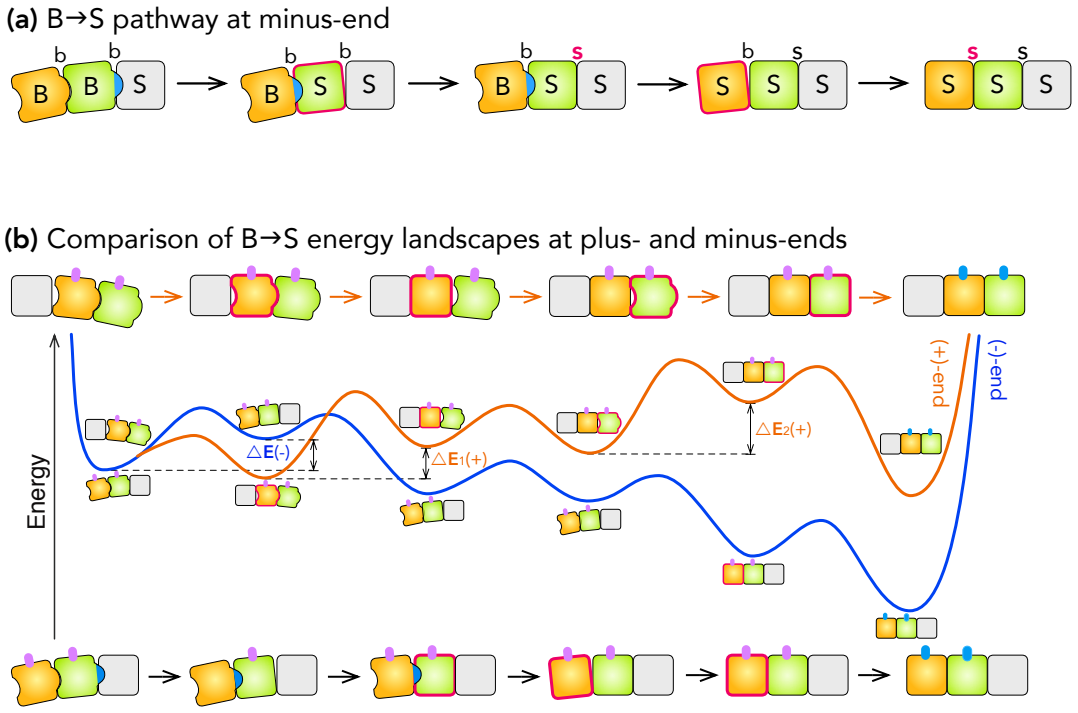

Figure S2: Kinetic pathway and EL for B→S transition at the minus-end. (**a**) The optimal kinetic pathway for B→S transition at minus-end. (**b**) Comparison of the ELs for B→S transitions at the plus- (Orange) and minus-end (Blue). There is only one major barrier $\Delta E(-)$ on the minus-end pathway but two major barriers $\Delta E_1(+)$ and $\Delta E_2(+)$ on the plus-end pathway.

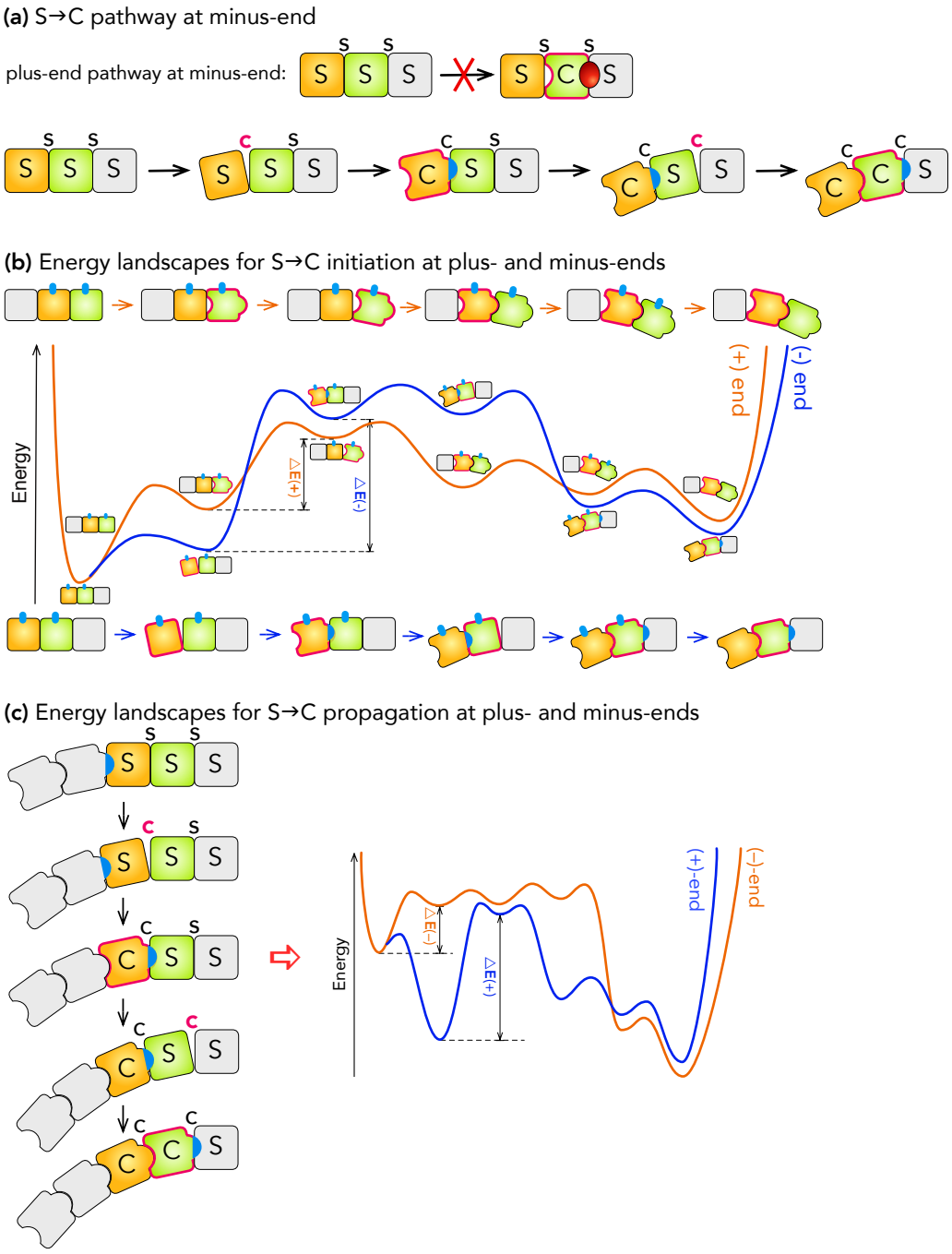

Figure S3: Kinetic pathway and ELs for S→C transition at the minus-end. (**a**) Schematics showing that the plus-end pathway (upper) for S→C transition leads to steric clashes at the minus-end, and the optimal pathway (lower) for the minus-end. (**b**) Comparison of the ELs for S→C initiation at the plus- (Orange) and the minus-end (Blue). (**c**) Comparison of the ELs for S→C propagation at the plus- (Orange) and the minus-end (Blue). The major barriers on plus- ($\Delta E(+)$) and minus-end ($\Delta E(-)$) pathways are marked respectively. The sequence of conformational changes in the S→C propagation at the minus-end is shown in the left.

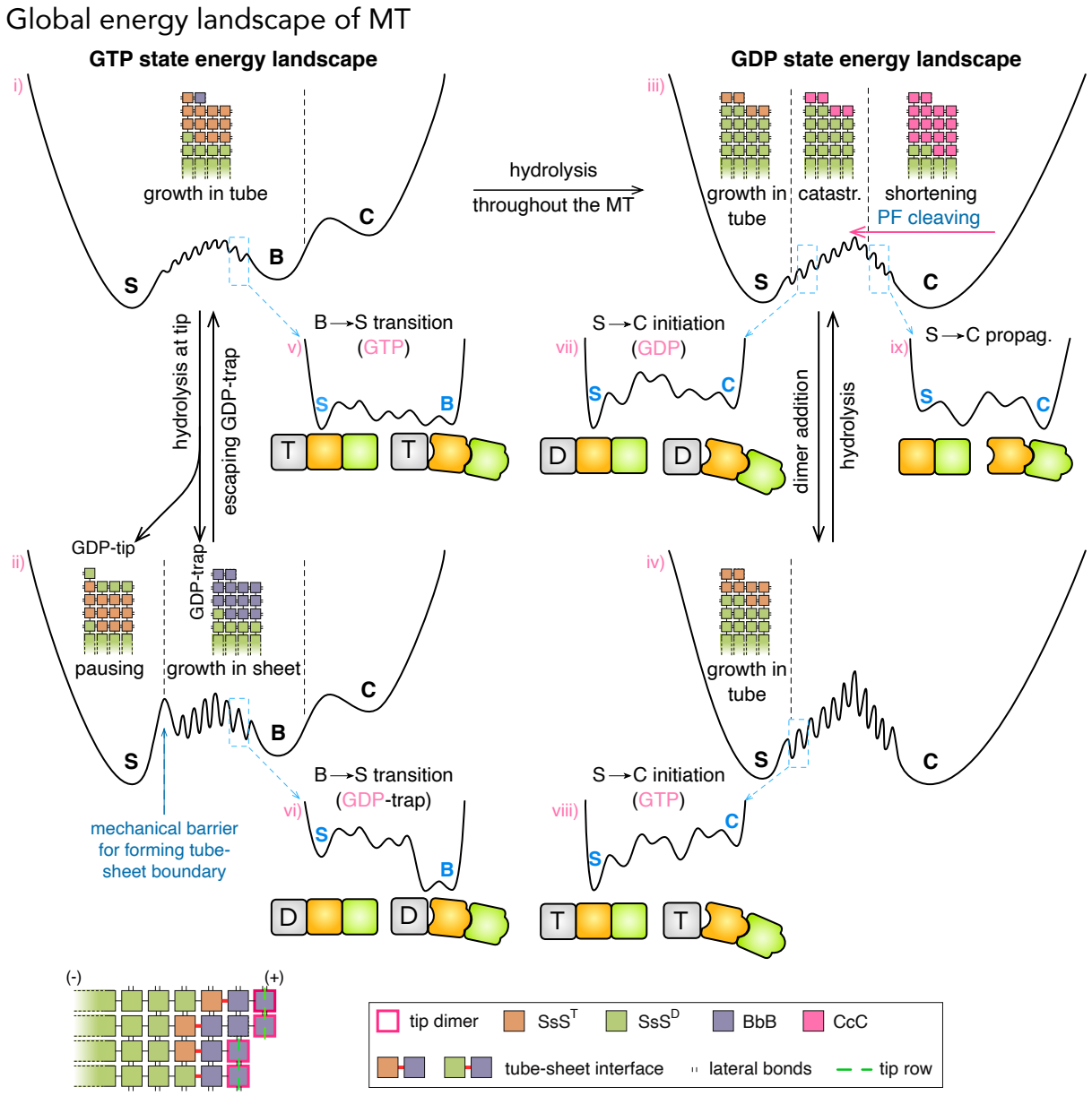

Figure S4: Schematics of the global (i–iv) and local (v–ix) energy landscapes of MT, and how their topologies change with the nucleotide state and lead to different phenomena of dynamic instability. Because of the lattice geometry of the MT, the global energy landscape is essentially a concatenation of the ELs for B→S→C transitions of the repeating units. Each small wiggle in the global energy landscapes is a coarse-grained representation of the energy landscape of a repeating unit that is shown in the zoomed-in insets (v, vi, vii, viii, ix), which are presented in detail in Figs. 5 and 6. The bottom shows the schematic of a MT lattice, with the terms (e.g. tip row, tip dimer) used in the Results section annotated.

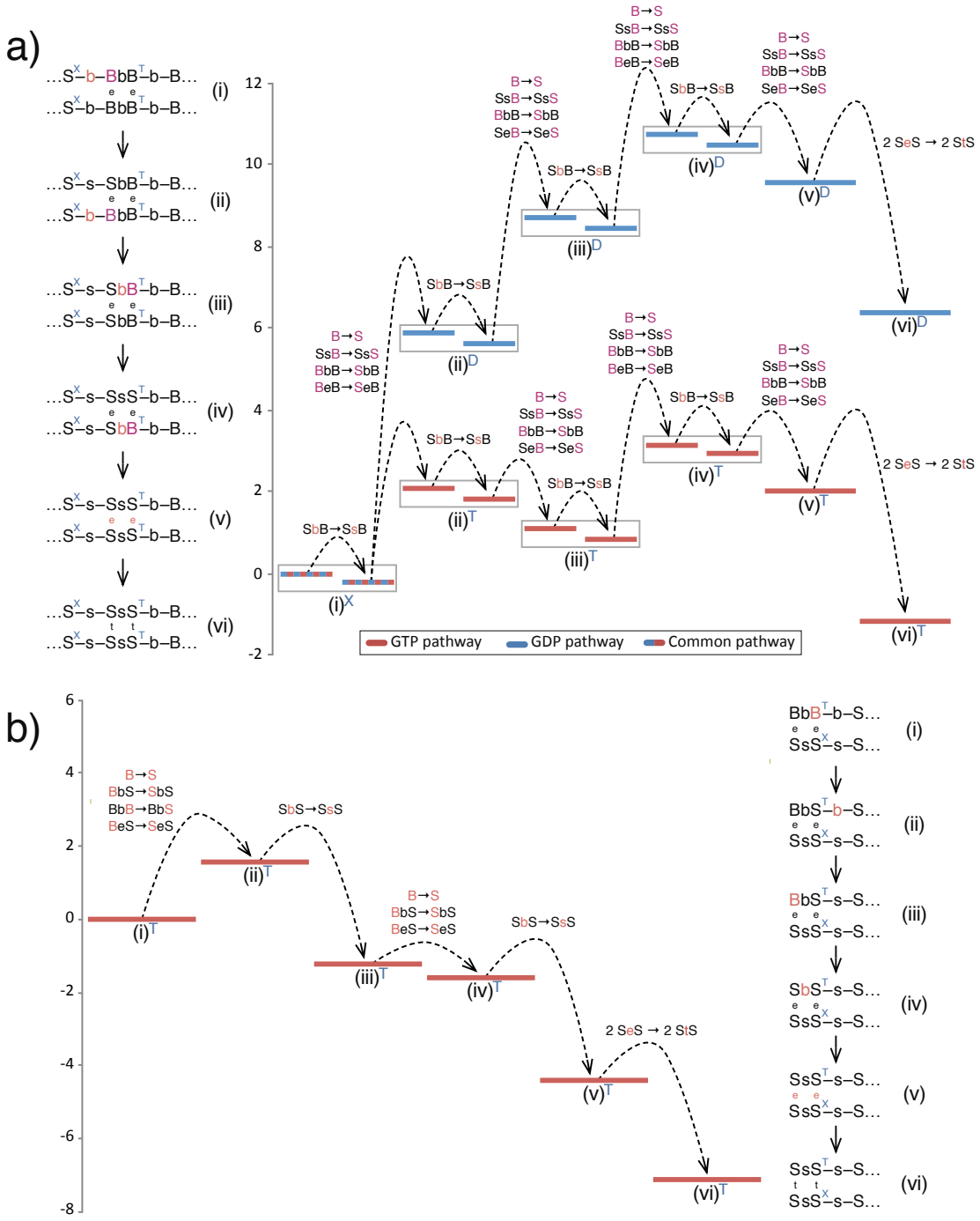

Figure S5: Optimal pathways and ELs for B→S transition. In a pathway, the right side denotes the plus-end side and the left side denotes the minus-end side; ⋯ denotes MT lattice omitted in a diagram. (**a**) B→S transition at plus-end with GTP (Blue) and GDP (Red) at the tube-sheet boundary respectively. (**b**) B→S transition at minus-end.

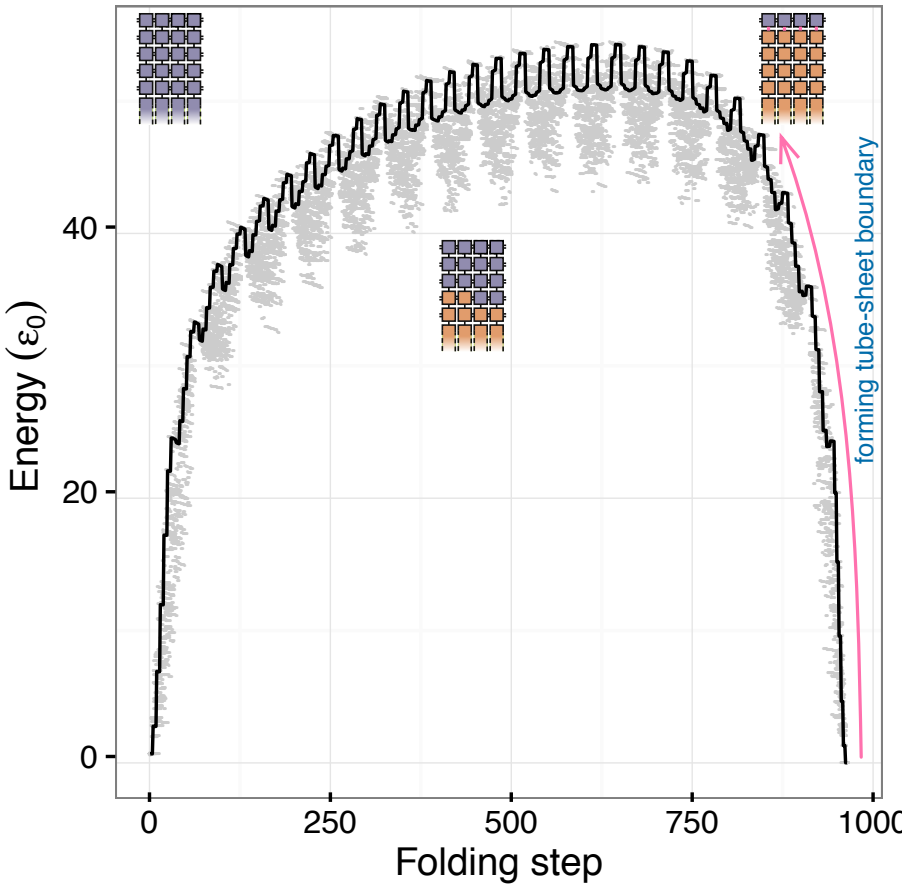

Figure S6: The mechanical energy profile for ribbon-to-tube transition of a 30-dimer MT. It was computed using the exact mechanical model. Each folding step corresponds to the B→S transition of a tubulin dimer or an inter-dimer longitudinal or lateral interface. The Black solid line denotes the mechanical energy change when the ribbon folds into tube by changing dimer and interface conformations from B to S in a strict row-by-row sequential order. Gray dots correspond to different orderings of the B→S transitions of dimers within the same row, which is stochastically determined to illustrate the variations in mechanical energy change with transition pathways. The region traced out by the Magenta arrow shows the mechanical energy cost of forming tube-sheet boundary.

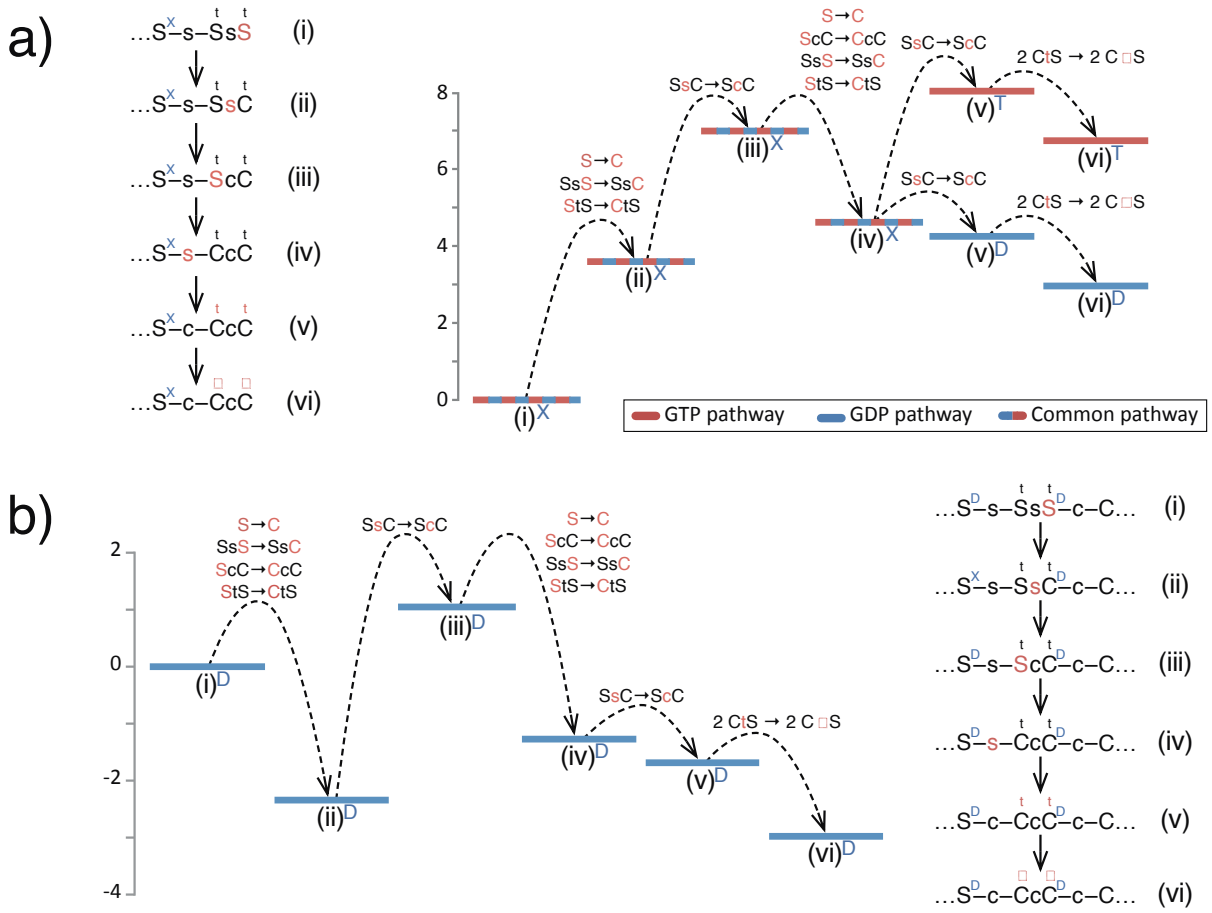

Figure S7: Optimal pathways and ELs for S→C transitions at plus-end. (**a**) S→C initiation with GTP and GDP behind the tip dimer respectively. (**b**) S→C propagation.

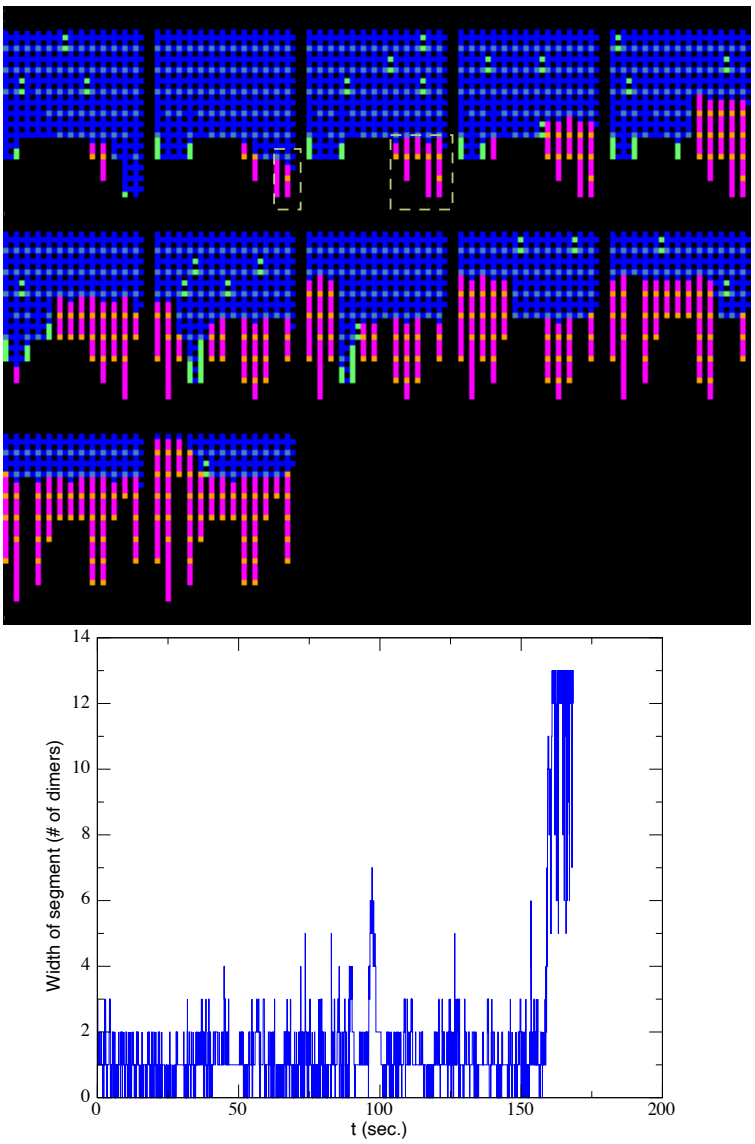

Figure S8: Events leading to a catastrophe in a trajectory at 10 μM tubulin concentration. (**upper**) Snapshots of the lattice states. The color code is the same as in Fig. S1. The two boxes in Green dashed lines in snapshots 2 and 3 indicate the formation and expansion of the stable catastrophe-nucleus that eventually leads to catastrophe. (**lower**) The width of the segment of curved tip dimers as a function of time in a trajectory that catastrophes in the end. Once the width exceeds 6 dimers, the chance to catastrophe is very high. The variation in segment width after catastrophe is due to PF cleaving.

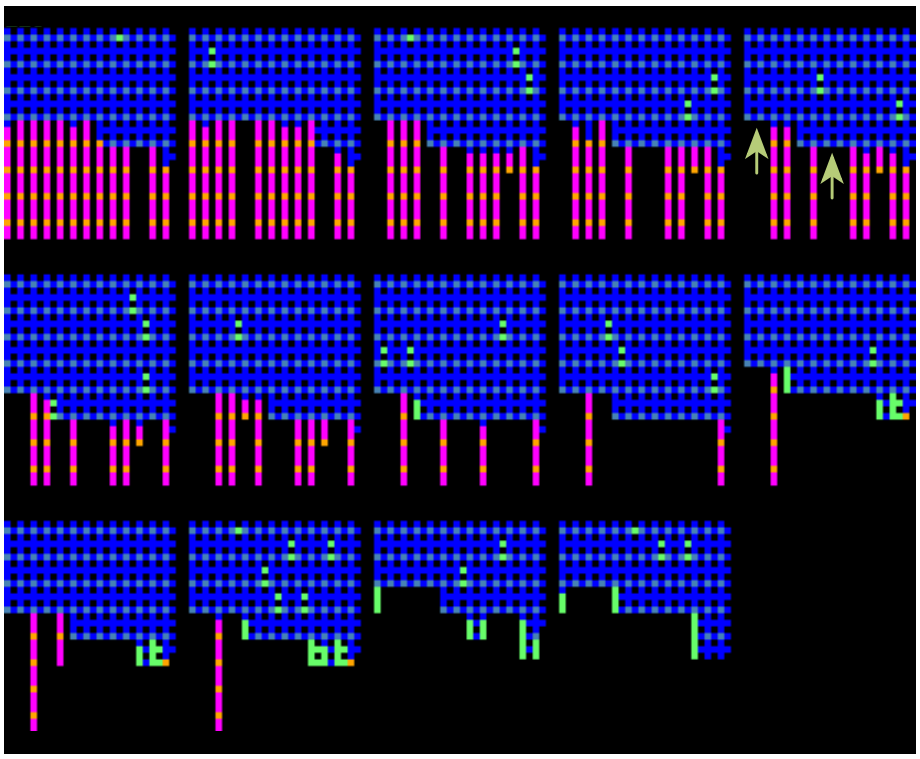

Figure S9: Snapshots of the lattice states that lead to a rescue event from a simulation at 10 μM tubulin concentration. The color code is the same as in Fig. S1. The two Green arrows in snapshot 5 indicate two rescue-nucleus that eventually leads to rescue.

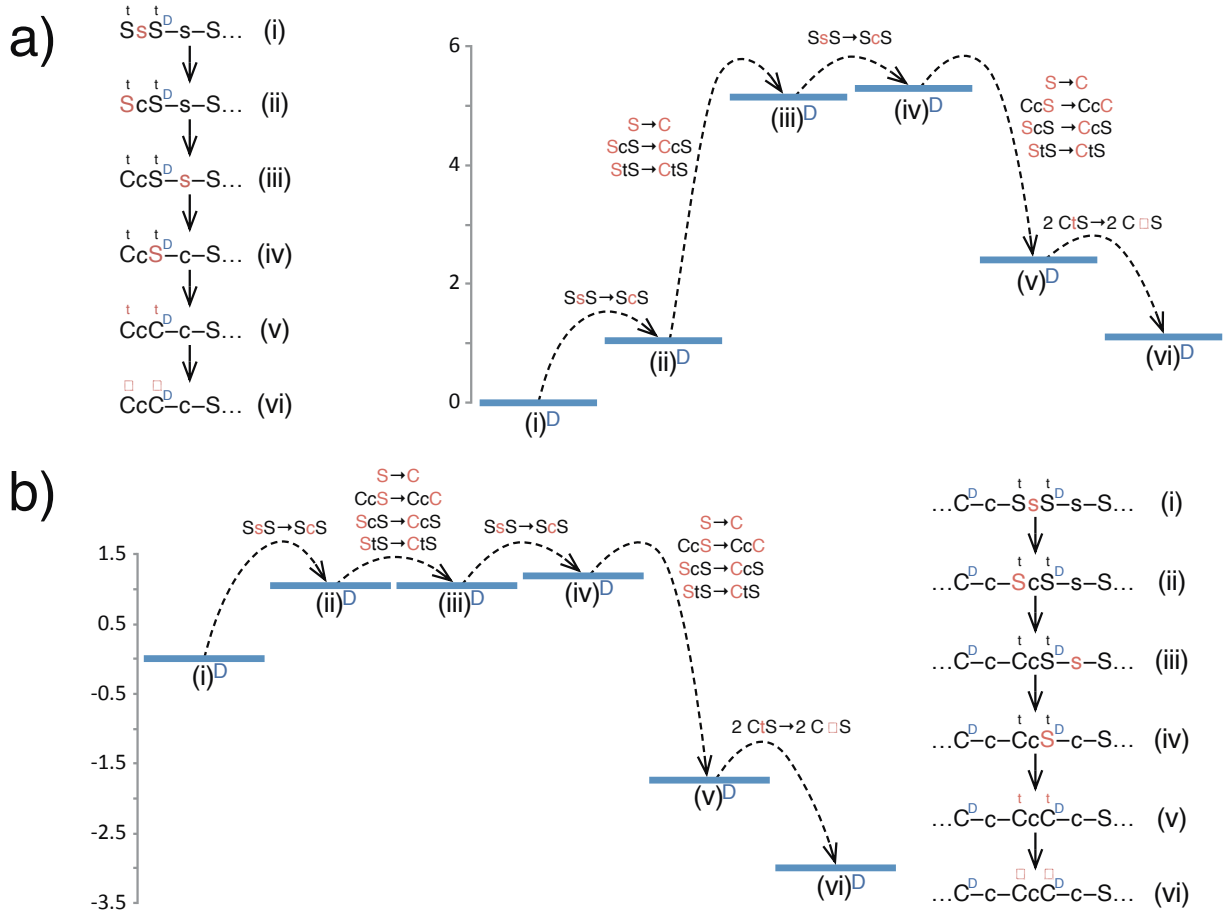

Figure S10: Optimal pathways and ELs for S→C transitions at minus-end. (**a**) S→C initiation with GTP and GDP behind the tip dimer respectively. (**b**) S→C propagation.

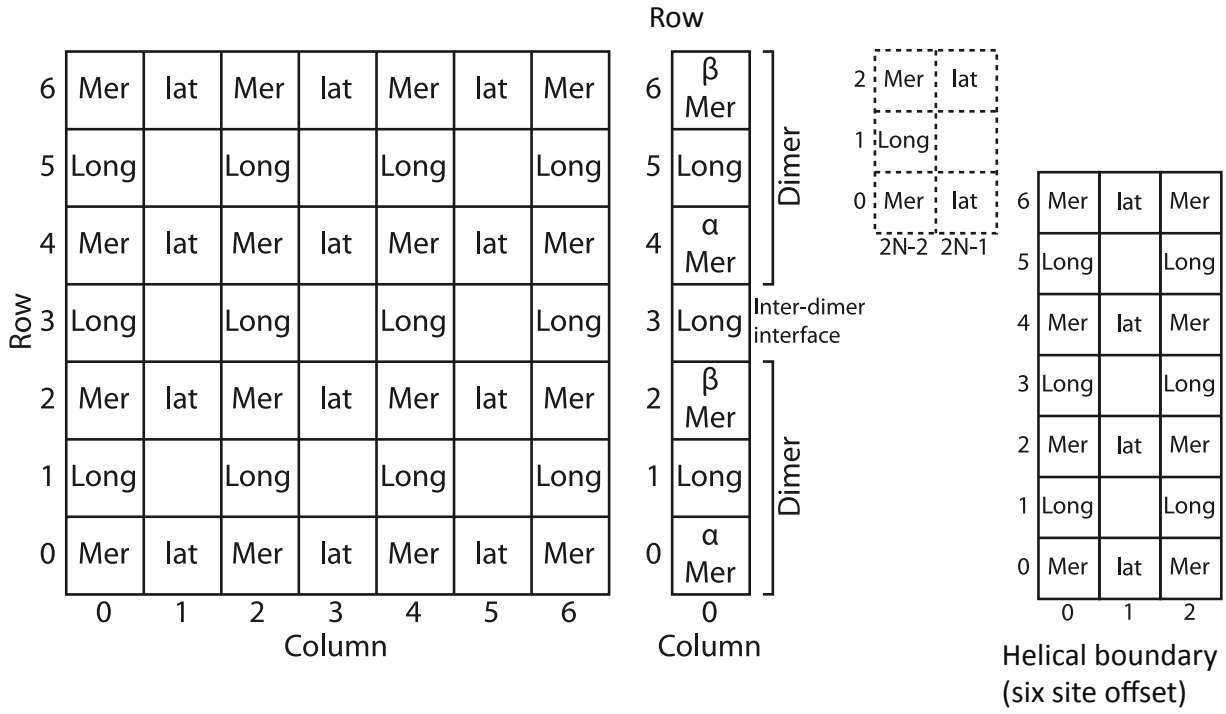

Figure S11: Schematic for the lattice for representing a microtubule used in the simulation. Mer: monomer (either α or β); Long: longitudinal interface; lat: lateral interface (details in section 3 of the SI).

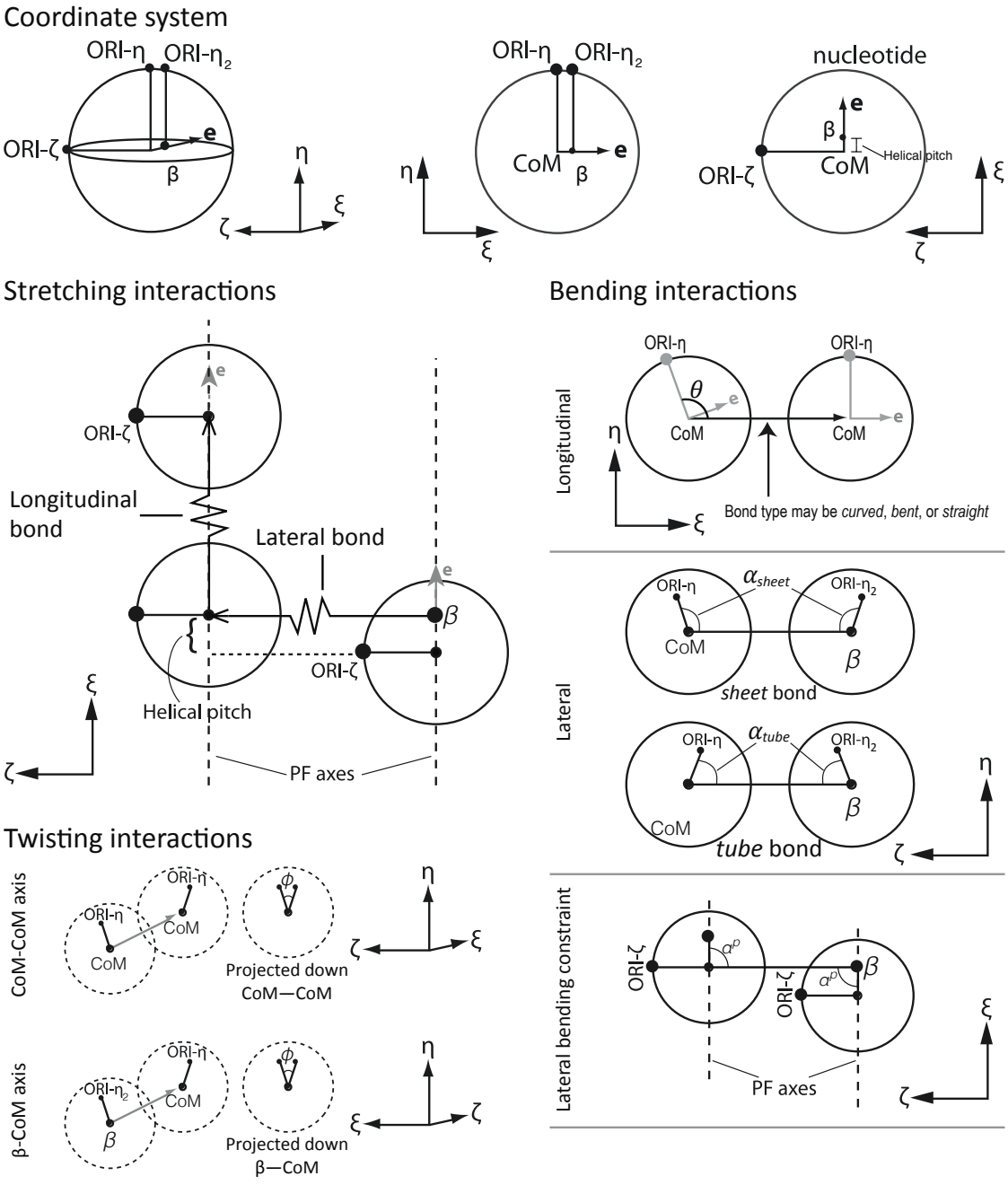

Figure S12: Schematics for the definitions of different terms in the full model for mechanical energy. The meaning of different symbols and terms are explained in STAR Methods text.

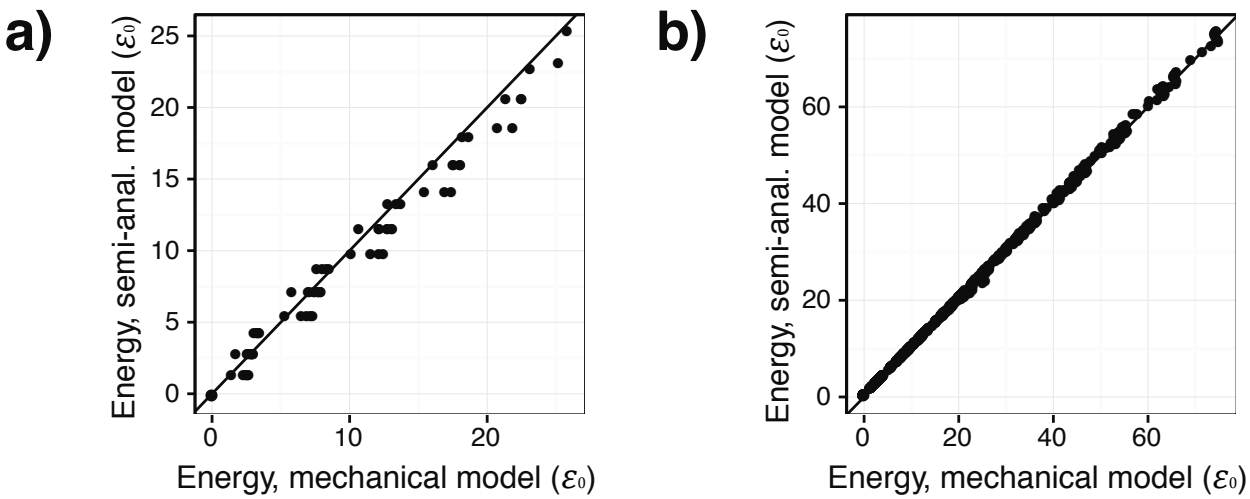

Figure S13: Comparison between mechanical energies calculated using the exact and semi-analytic model. (**a**) The change in mechanical energy from adding one additional row of sheet with different offsets. (**b**) The strain retention energy.

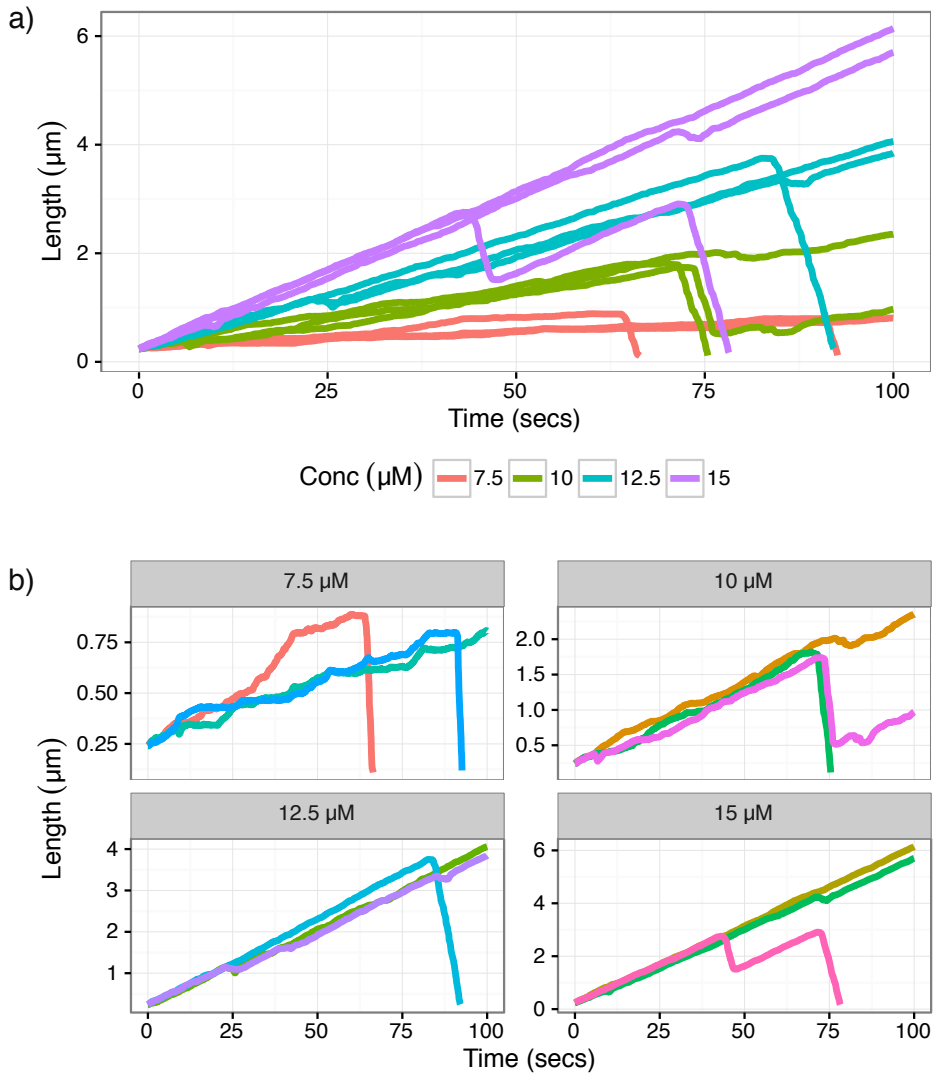

Figure S14: Sample trajectories of microtubule assembly from simulations at different concentrations. (**a**) Comparison of trajectories from different concentrations. (**b**) Detailed features of sample trajectories for each concentration.

Parameter	Rate
k_{mer}	$1.0 \times 10^5\ s^{-1}$
k_{long}	$0.5 \times 10^5\ s^{-1}$
k_{lat}	$0.175 \times 10^5\ s^{-1}$
k_{as}	$12.5\ \mu M^{-1} \cdot s^{-1}$
k_{off}	$4.0 \times 10^5\ s^{-1}$
k_{hyd}	$5.0\ s^{-1}$

Table S1: Prefactors for different reaction types, related to STAR Methods.

Parameter	Value
k_{long}	$5000\ \epsilon_0/L_0^2$
k_{lat}	$250\ \epsilon_0/L_0^2$
k_θ	$20.0\ \epsilon_0/\mathrm{rad}^2$
k_α	$25.0\ \epsilon_0/\mathrm{rad}^2$
k_ϕ	$5.0\ \epsilon_0$

Table S2: Parameters for the full mechanical model, related to STAR Methods. ($L_0 = 4nm, \epsilon_0 = k_BT = 0.616\ kcal/mol$, k_B is the Boltzmann constant)

Parameter	Value
a	-1.541
b	2.837
c	-0.096
d	1.331
p	0.145

Table S3: Parameters of the single-row fit for the semi-analytic model, related to STAR Methods.

Width (PFs)	*r*	σ no tube	σ left tube	σ right tube	σ both tube
1	0.0000	0.0000	0.0766	0.0765	0.1320
2	0.0001	0.0091	0.1438	0.1522	0.1282
3	0.0679	0.0000	0.2145	0.1631	0.2588
4	0.0860	0.0142	0.2985	0.2844	0.2002
5	0.1552	0.0123	0.3607	0.2276	0.3189
6	0.2849	0.0000	0.4140	0.3421	0.2001
7	0.3398	0.0000	0.4611	0.2208	0.2463
8	0.4461	0.0000	0.3887	0.2784	0.1278
9	0.4973	0.0000	0.4240	0.1458	0.1980
10	0.5748	0.0000	0.3037	0.2113	0.1508
11	0.6122	0.0000	0.3314	0.1615	0.0335
12	0.6610	0.0000	0.0174	0.0127	0.0335
13	0.6873	0.0000	0.0174	0.0127	0.0335

Table S4: Strain retention ratio and lateral strain parameters for the semi-analytic model, related to STAR Methods.